

## OPTICAL AND INFRARED COLORS OF STARS OBSERVED BY THE TWO MICRON ALL SKY SURVEY AND THE SLOAN DIGITAL SKY SURVEY<sup>1</sup>

KRISTIAN FINLATOR,<sup>2</sup> ŽELJKO IVEZIĆ,<sup>2</sup> XIAOHUI FAN,<sup>2</sup> MICHAEL A. STRAUSS,<sup>2</sup> GILLIAN R. KNAPP,<sup>2</sup> ROBERT H. LUPTON,<sup>2</sup> JAMES E. GUNN,<sup>2</sup> CONSTANCE M. ROCKOSI,<sup>3</sup> JOHN E. ANDERSON,<sup>4</sup> ISTVÁN CSABAI,<sup>5,6</sup> GREGORY S. HENNESSY,<sup>7</sup> ROBERT B. HINDSLEY,<sup>8</sup> TIMOTHY A. MCKAY,<sup>9</sup> ROBERT C. NICHOL,<sup>10</sup> DONALD P. SCHNEIDER,<sup>11</sup> J. ALLYN SMITH,<sup>9</sup> AND DONALD G. YORK<sup>3</sup> (FOR THE SDSS COLLABORATION)

Received 2000 June 8; accepted 2000 July 31

### ABSTRACT

We discuss optical and infrared photometric properties of stars matched in the Two Micron All Sky Survey (2MASS) and the Sloan Digital Sky Survey (SDSS) commissioning data for  $\sim 50$  deg<sup>2</sup> of sky along the celestial equator centered at  $l = 150^\circ$ ,  $b = -60^\circ$ . About 98% ( $\sim 63,000$ ) of objects listed in the 2MASS Point Source Catalog in the analyzed area are matched within  $2''$  to an SDSS source. The matched sources represent 8% of the  $\sim 800,000$  SDSS sources in this area. They are predominantly red sources, as expected, and 15% of them are resolved in SDSS imaging data although they are detected as point sources in 2MASS data. The distribution of positional discrepancies for the matched sources and the astrometric statistics for the multiply observed SDSS sources imply that the astrometric accuracy of both surveys is about 0.1 per coordinate (rms). For about 14,000 stars with the smallest photometric errors ( $\lesssim 10\%$ ) in both surveys, we present optical and infrared color-magnitude and color-color diagrams. We use optical (SDSS) colors to identify the stellar spectral sequence and show that stars of different spectral types can have similar infrared colors, thus making the classification of stars based on only 2MASS data very difficult. However, a broad separation into “early” and “late” spectral types (relative to type K0) is possible with a reliability of  $\sim 95\%$  even with 2MASS colors alone. The distributions of matched sources in color-magnitude and color-color diagrams are compared with the predictions of a stellar population synthesis code. We find that the models are in fair overall agreement with the data. In particular, the total number counts agree to better than 10%, and the morphologies of the color-magnitude and color-color diagrams appear similar. The most significant discrepancies are found for the number ratio of “early” to “late” type stars (by about a factor of 2) and in the colors of M stars (up to 0.2 mag). The first disagreement indicates that some parameters of the standard Galactic structure model and/or initial mass function can be improved, and the second disagreement emphasizes known difficulties with the modeling of stellar atmospheres for cool stars.

*Key words:* Galaxy: stellar content

### 1. INTRODUCTION

The Two Micron All Sky Survey (2MASS; Skrutskie et al. 1997) and the Sloan Digital Sky Survey (SDSS; York et al. 2000) are producing eight-color optical and infrared photometry for millions of Galactic and extragalactic sources. It is of obvious scientific interest to positionally match the

sources observed in both surveys and to study their distribution in color-magnitude and color-color diagrams. Due to the large number of sources and very accurate photometry and astrometry, such a study can, for example, reliably reveal detailed properties of “normal” stars, which should constitute the majority of matched sources. This information is invaluable for studying stellar and Galactic structure and evolution, and it also makes feasible efficient searches for peculiar or previously unknown objects. For example, the selection of recently defined L dwarfs (Kirkpatrick et al. 1999) was based on both optical and infrared photometry, an approach still followed in the current searches for L and T dwarfs (e.g., Leggett et al. 2000).

In this paper we present preliminary results for matched sources from the recent 2MASS Second Incremental Data Release<sup>12</sup> and SDSS commissioning data. A brief description of both surveys is provided in § 2. We describe the matching and the basic statistics in § 3. A more detailed study of optical-infrared properties of stars is presented in § 4, and in § 5 we compare data with models.

<sup>1</sup> Based on observations obtained with the Sloan Digital Sky Survey.

<sup>2</sup> Princeton University Observatory, Princeton, NJ 08544.

<sup>3</sup> University of Chicago, Astronomy and Astrophysics Center, 5640 South Ellis Avenue, Chicago, IL 60637.

<sup>4</sup> Fermi National Accelerator Laboratory, P.O. Box 500, Batavia, IL 60510.

<sup>5</sup> Department of Physics and Astronomy, Johns Hopkins University, 3701 San Martin Drive, Baltimore, MD 21218.

<sup>6</sup> Department of Physics of Complex Systems, Eötvös University, Pázmány Péter sétány 1/A, Budapest, H-1117, Hungary.

<sup>7</sup> US Naval Observatory, 3450 Massachusetts Avenue NW, Washington, DC 20392-5420.

<sup>8</sup> Remote Sensing Division, Code 7215, Naval Research Laboratory, 4555, Overlook Avenue SW, Washington, DC 20375.

<sup>9</sup> Department of Physics, University of Michigan, 500 East University, Ann Arbor, MI 48109.

<sup>10</sup> Department of Physics, Carnegie Mellon University, 5000 Forbes Avenue, Pittsburgh, PA 15232.

<sup>11</sup> Department of Astronomy and Astrophysics, Pennsylvania State University, University Park, PA 16802.

<sup>12</sup> Available at <http://www.ipac.caltech.edu/2mass/releases/second/index.html>.

## 2. THE DATA

## 2.1. 2MASS

The 2MASS is using two 1.3 m telescopes, one on Mt. Hopkins in Arizona and one at the Cerro Tololo Inter-American Observatory (CTIO) in Chile, to survey the entire sky in near-infrared light.<sup>13</sup> The northern telescope has been observing regularly since 1997 June, while the southern facility began operation in 1998 March. Each telescope's camera is equipped with three  $256 \times 256$  arrays (the pixel size is  $2''$ ) of HgCdTe detectors and observes simultaneously in the  $J$  ( $1.25 \mu\text{m}$ ),  $H$  ( $1.65 \mu\text{m}$ ), and  $K_s$  ( $2.17 \mu\text{m}$ ) bands. The detectors are sensitive to point sources brighter than about 1 mJy at the  $10 \sigma$  level, corresponding to limiting (Vega-based) magnitudes of 15.8, 15.1, and 14.3, respectively. Point-source photometry is repeatable to better than 10% precision at this level, and the astrometric uncertainty for these sources is less than  $0''.2$ .

When completed, 2MASS will catalog  $\sim 300$  million stars, as well as several million galaxies, and will cover at least 95% of the sky. A new data installment, the 2MASS Second Incremental Data Release, was recently made available to the public. Spanning 47% of the sky, it contains

photometry and astrometry for over 162 million point sources as well as 1.9 million resolved sources.

## 2.2. SDSS

The SDSS is a digital photometric and spectroscopic survey which will cover one quarter of the celestial sphere in the northern Galactic cap and produce a smaller area ( $\sim 225 \text{ deg}^2$ ) but much deeper survey in the southern Galactic hemisphere (York et al. 2000<sup>14</sup>). The flux densities of detected objects are measured almost simultaneously in five bands ( $u'$ ,  $g'$ ,  $r'$ ,  $i'$ , and  $z'$ ; Fukugita et al. 1996) with effective wavelengths of 3540, 4760, 6280, 7690, and 9250 Å, 95% complete<sup>15</sup> for point sources to limiting magnitudes of 22.1, 22.4, 22.1, 21.2, and 20.3 in the northern Galactic cap.<sup>16</sup> The survey sky coverage of about  $\pi$  steradians ( $10,000 \text{ deg}^2$ ) will

<sup>14</sup> See also <http://www.astro.princeton.edu/PBOOK/welcome.htm>.

<sup>15</sup> These values are determined by comparing multiple scans of the same area obtained during the commissioning year. Typical seeing in these observations was  $1''.5 \pm 0''.1$ .

<sup>16</sup> We refer to the measured magnitudes in this paper as  $u^*$ ,  $g^*$ ,  $r^*$ ,  $i^*$ , and  $z^*$  because the absolute calibration of the SDSS photometric system is still uncertain at the  $\sim 0.03$  mag level. The SDSS filters themselves are referred to as  $u'$ ,  $g'$ ,  $r'$ ,  $i'$ , and  $z'$ . All magnitudes are given on the AB<sub>s</sub> system (Oke & Gunn 1983; for additional discussion regarding the SDSS photometric system see Fukugita et al. 1996 and Fan 1999).

<sup>13</sup> See <http://www.ipac.caltech.edu/2mass/overview/about2mass.html>.

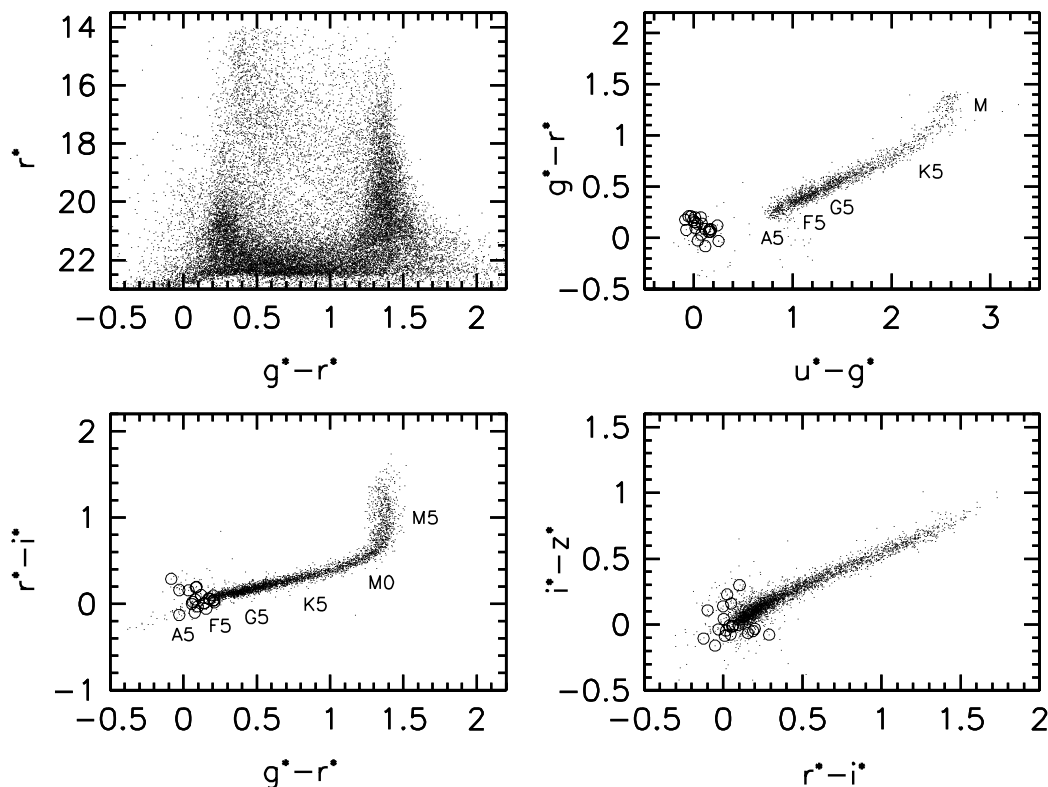


FIG. 1.—SDSS color-color and color-magnitude diagrams, which summarize photometric properties of unresolved sources, marked as dots. The top left panel displays an  $r^*$  vs.  $g^*-r^*$  color-magnitude diagram for  $\sim 25,000$  objects observed in  $3 \text{ deg}^2$  of sky during SDSS commissioning run 94. The three remaining panels show color-color diagrams for objects brighter than 20 mag in each of the three bands used to construct each diagram (*red is always toward the upper right corner*). The locus of “normal” stars is clearly visible in all three diagrams, and the positions of several spectral types are indicated next to the locus in the  $u^*-g^*$  vs.  $g^*-r^*$  and  $r^*-i^*$  vs.  $g^*-r^*$  color-color diagrams. Objects that have  $u^*-g^*$  and  $g^*-r^*$  colors similar to low-redshift QSOs ( $u^*-g^* < 0.4$ ,  $-0.1 < g^*-r^* < 0.3$ ,  $r^*-i^* < 0.5$ ) and are brighter than the limit for quasars in the SDSS spectroscopic survey ( $i^* < 19$ ) are marked by open circles. See the electronic edition of the *Journal* for a color version of this figure.

result in photometric measurements to the above detection limits for about 50 million stars. Astrometric positions are accurate to about 0.1 per coordinate for sources brighter than  $r^* \sim 20.5$  mag, and the morphological information from the images allows robust star-galaxy separation to  $r^* \sim 21.5$  mag.

### 3. MATCHED DATA

#### 3.1. SDSS Data

We utilize a portion of SDSS imaging data from two commissioning runs (numbered 94 and 125) taken during the fall of 1998. The data in each run were obtained in six parallel scan lines,<sup>17</sup> each 13.5 wide, along the Celestial Equator ( $-1.2687 < \delta_{J2000.0} < 1.2676$ ). The six scan lines from each run are interleaved to make a filled stripe. The portion of data used in this work extends from  $\alpha_{J2000.0} = 0^h 24^m$  ( $l = 108^\circ$ ,  $b = -62^\circ$ ) to  $\alpha_{J2000.0} = 3^h 0^m$  ( $l = 177^\circ$ ,  $b = -49^\circ$ ). The seeing in both runs was variable between 1" and 2" (FWHM) with the median value typically 1.5". The total area which overlaps with public 2MASS data is 47.41 deg<sup>2</sup> and includes about 800,000 SDSS sources to the  $6\sigma$  detection limit in at least one of the SDSS bands.

The SDSS color-color and color-magnitude diagrams that summarize photometric properties of unresolved sources are shown in Figure 1. In this and all other figures, we correct the data for the interstellar extinction<sup>18</sup> deter-

mined from the maps given by Schlegel, Finkbeiner, & Davis (1998). Typical values for high-latitude regions discussed in this work are  $A_{r^*} = 0.05$ – $0.15$  mag ( $A_{r^*} = 0.84A_V$ ). Throughout this work we use the point-spread function (PSF) magnitudes<sup>19</sup> (measured by fitting a PSF model of a double Gaussian and applying an aperture correction) as computed by the photometric pipeline (PHOTO, version v5\_0; for details see Lupton et al. 2000). Photometric errors are typically 0.03 mag at the bright end ( $r^* < 20$  mag) relevant in this work (for more details see Ivezić et al. 2000).

The top left panel of Figure 1 displays the  $r^*$  versus  $g^* - r^*$  color-magnitude diagram for  $\sim 25,000$  objects observed in 3 deg<sup>2</sup> of sky during SDSS commissioning run 94. There are at least three distinct groups of sources. The red sources with  $g^* - r^* \sim 1.4$  are disk stars and are dominated by stars of spectral type M; see e.g., Fukugita et al. (1996) and Lenz et al. (1998). The blue ridge with  $g^* - r^* \sim 0.4$  is dominated by F and G disk stars at the bright end ( $r^* \lesssim 18$ ) and by halo stars at the faint end (note that the median  $g^* - r^*$  color for halo stars is bluer than for disk stars, due to the lower metallicity in the halo). As shown by Fan (1999), the contribution of low-redshift ( $z \lesssim 2$ ) quasars (QSOs) becomes increasingly important at the faint end of the blue ridge. The majority of stars observed by SDSS are on main sequence; with the aid of models discussed in § 5 we estimate that the fraction of stars which are not on main sequence is  $\sim 1.0\%$ . The latter are dominated

<sup>17</sup> See also <http://www.astro.princeton.edu/PBOOK/strategy/strategy.htm>.

<sup>18</sup> The Galactic structure model discussed in § 5 implies that the most sources in this sample are further than 200 pc away, which justifies this correction.

<sup>19</sup> Note that SDSS photometric system uses asinh magnitudes (Lupton, Gunn, & Szalay 1999). For reference, zero flux corresponds to asinh magnitudes of 23.40, 24.22, 23.98, 23.51, and 21.83 in  $u^*$ ,  $g^*$ ,  $r^*$ ,  $i^*$ , and  $z^*$ , respectively.

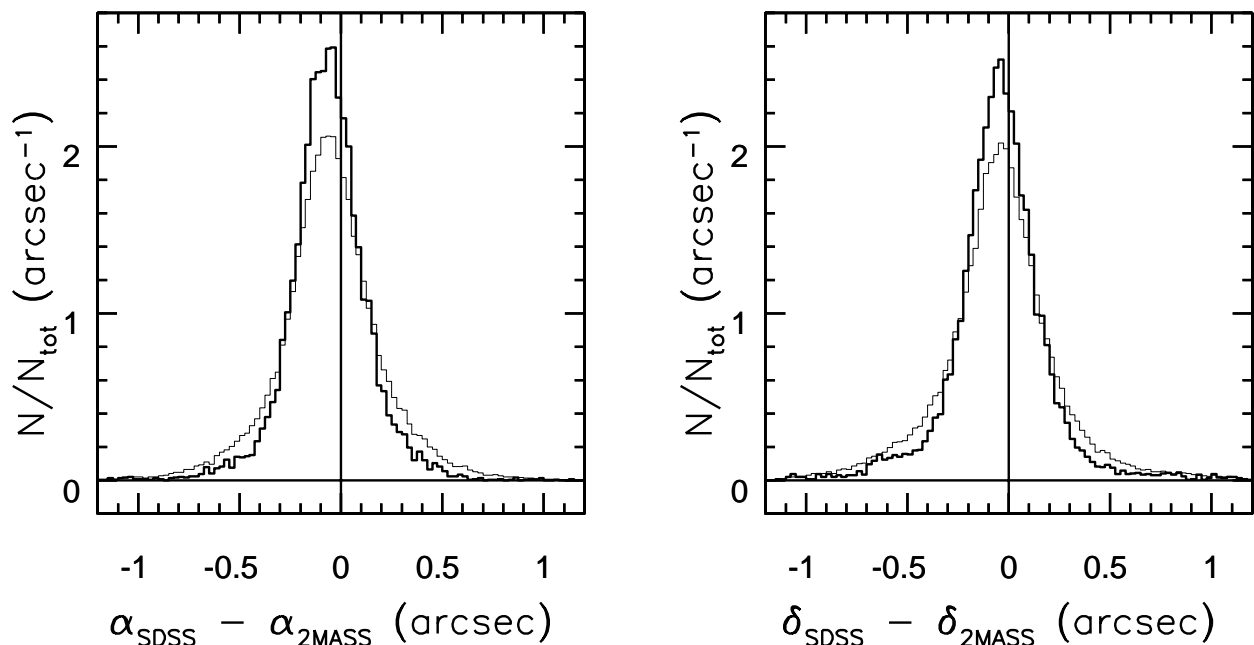


FIG. 2.—Probability distributions of right ascension and declination differences between the SDSS and 2MASS positions. The thin lines show the normalized histograms for all matched sources ( $\sim 63,000$ ) and the thick lines show histograms for  $\sim 14,000$  sources with the highest S/N (see text). The equivalent Gaussian widths determined from the interquartile range are 0.30 for the distributions of all sources and 0.15 for the high-S/N sources. Note that the histograms show a 0.05 offset from the origin in both coordinates. This appears to be a systematic effect in the SDSS astrometry (see text). See the electronic edition of the *Journal* for a color version of this figure.

by giants and subgiants with  $0.4 < g^* - r^* < 0.8$  ( $\sim 90\%$ ) and horizontal branch stars with  $g^* - r^* < 0.5$  ( $\sim 10\%$ ).

The three remaining panels show three projections of the SDSS color-color diagrams for objects, marked as dots, brighter than 20 mag in each of the three bands used to construct each diagram. Red is always toward the upper right corner. Objects that have  $u^* - g^*$  and  $g^* - r^*$  colors similar to low-redshift QSOs ( $u^* - g^* < 0.4$ ,  $-0.1 < g^* - r^* < 0.3$ ,  $r^* - i^* < 0.5$ ) and are brighter than the limit for quasars in the SDSS spectroscopic survey ( $i^* < 19$ ) are marked by open circles.

The locus of “normal” stars stands out in all three diagrams. As shown by Fukugita et al. (1996), Krisciunas, Margon, & Szkody (1998), Lenz et al. (1998), and Fan (1999), the position of a star in these diagrams is mainly determined by its spectral type. For reference, the positions of several spectral types taken from Fukugita et al. (1996) are marked next to the stellar locus in the  $u^* - g^*$  versus  $g^* - r^*$  and  $r^* - i^*$  versus  $g^* - r^*$  color-color diagrams (labels are slightly offset for clarity).

For most of its length, the locus in the  $g^* - r^*$  versus  $u^* - g^*$  diagram is made of stars with spectral types ranging from F to late K. A-type stars are visible at  $u^* - g^* \sim 1.0$ – $1.2$  and  $g^* - r^* \sim -0.3$ – $0.0$  (for a detailed study of A stars detected in SDSS commissioning data see Yanny et al. 2000), and late-K and M stars are found at the red end of the stellar locus. Different M spectral subtypes cannot be distinguished in the  $g^* - r^*$  versus  $u^* - g^*$  diagram, and these stars are better separated in the  $r^* - i^*$  versus  $g^* - r^*$  diagram. M stars have a constant  $g^* - r^*$  color ( $\sim 1.4$ ) due to strong TiO bands in their spectra and a value of  $r^* - i^*$  color that depends strongly on spectral subtype. In the  $i^* - z^*$  versus  $r^* - i^*$  diagram, stars earlier than K type are found in a small region around  $r^* - i^* \sim 0.2$  and  $i^* - z^* \sim 0.0$ . For most of its length, the  $i^* - z^*$  versus  $r^* - i^*$  stellar locus represents late K and M stars.

### 3.2. 2MASS Data

We positionally match data from the two SDSS commissioning runs to 2MASS Point Source Catalog (PSC) data with  $0^{\text{h}}24^{\text{m}} < \alpha_{J2000.0} < 3^{\text{h}}0^{\text{m}}$  and  $-1^{\circ}26'87'' < \delta_{J2000.0} < 0^{\circ}$  (2MASS data for  $0^{\circ} < \delta_{J2000.0} < 1^{\circ}26'76''$  are not yet available). The region with  $1^{\text{h}}51^{\text{m}} < \alpha_{J2000.0} < 1^{\text{h}}57^{\text{m}}$  is missing from the 2MASS catalog. The resulting overlapping area ( $47.41 \text{ deg}^2$ ) includes 64,695 2MASS sources.

### 3.3. The Positional Matching of SDSS and 2MASS Catalogs

We consider as matches all sources from both catalogs whose listed positions agree to better than  $2''$ . There are 63,341 such sources, or 97.9% of the 2MASS PSC sources and 8% of the SDSS sources, in the overlapping area. The probability of finding an SDSS source within a circle with  $2''$  radius is  $\sim 1\%$ , and the probability of associating a 2MASS source with multiple SDSS sources is thus negligible ( $< 10^{-4}$ ). With the further constraints on the final sample, discussed in § 4, the random association rate for matched sources also becomes inconsequential ( $< 10^{-5}$ ).

The distributions of right ascension and declination differences between the SDSS and 2MASS catalog positions are shown in Figure 2. The thin lines show the normalized histograms for all matched sources, and the thick lines show histograms for the  $\sim 14,000$  sources with at least  $10\sigma$  detections in both surveys (see the next section), which are not

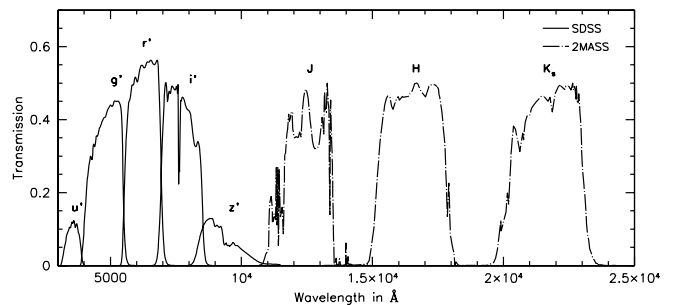


FIG. 3.—SDSS and 2MASS bandpasses. The five solid curves correspond to the overall SDSS efficiencies, and the three dot-dashed lines show the 2MASS responses normalized to 0.5 at the peak value. All curves include typical atmospheric extinction and the transmission of the entire instrumental system. See the electronic edition of the *Journal for a color version of this figure*.

saturated or blended with other sources in the SDSS images. Both histograms are normalized by the total number of sources. Equivalent Gaussian widths determined from the interquartile range are  $0''.30$  for the distributions of all sources and  $0''.15$  for the sources with the high signal-to-noise ratio (S/N).<sup>20</sup> As the multiple SDSS commissioning observations of the same area show that the positions of sources with high S/N are reproducible to  $0''.10$  per coordinate (Pier et al. 2000), this implies that the astrometric accuracy of both 2MASS and SDSS is about  $0''.10$  for bright sources (positional rms scatter per coordinate). However, note that the histograms displayed in Figure 2 show a  $0''.05$  offset from the origin for both coordinates. A comparison of the SDSS and VLA FIRST Survey (Becker et al. 1995)<sup>21</sup> data shows the same offset (though with less statistical significance due to the smaller number of matched sources), indicating that this is a systematic error in the SDSS astrometry. We are currently investigating this problem.

### 3.4. Unmatched 2MASS PSC Sources

There are 1354 2MASS sources (2.1% of the whole sample) that do not have a cataloged SDSS source within  $2''$ . Visual inspection of SDSS images shows that 70% of these do not have an optical counterpart at the cataloged 2MASS position. Such sources are either spurious 2MASS detections (roughly 80% of the unmatched 2MASS sources have  $S/N < 10$  in all 2MASS bands), extremely red sources (e.g., stars heavily obscured by circumstellar dust), or asteroids that moved between the times of the SDSS and 2MASS observations. There is no significant correlation between the number of unmatched sources and the distance from the ecliptic plane.

Of the unmatched 2MASS sources, 15% are associated in SDSS images with saturated stars. The centroids of saturated stars in SDSS have a large positional uncertainty, which sometimes may exceed the matching cutoff  $2''$ . 10% of the unmatched 2MASS sources are associated in SDSS images

<sup>20</sup> The contribution of the proper motions to this scatter is negligible because of the short time span between the SDSS and 2MASS observations.

<sup>21</sup> See also Faint Images of the Radio Sky at Twenty Centimeters at <http://sundog.stsci.edu/>.

with complex structures consisting of several blended sources, and which were not deblended by the processing software. The remaining 5% of the unmatched sources are blended with a satellite trail or a diffraction spike of a nearby bright star in the SDSS data. This category represents only 0.1% of the total number of 2MASS sources.

#### 4. OPTICAL AND INFRARED PROPERTIES OF STELLAR SOURCES

The combined SDSS and 2MASS eight-color photometry can be used to construct a multitude of point source color-magnitude and color-color diagrams. The five SDSS and three 2MASS bandpasses are shown in Figure 3. All curves include typical atmospheric extinction and the transmission of the entire instrumental system. The solid curves correspond to the overall efficiencies of the SDSS system (Gunn et al. 1998), and the dot-dashed lines show the 2MASS responses normalized to 0.5 (M. Cohen 2000, private communication).

Since the thrust of this work is to provide the accurate optical and infrared colors of normal stars, we apply several conditions on the matched sources in order to select a subsample of stars with the best photometric data.

1. The 2MASS and SDSS positions must agree to better than  $1''$ . This limit corresponds to a  $\sim 5\sigma$  cut.

2. Sources must not be saturated in any band in the SDSS data. This is roughly equivalent to the condition  $i^* > 14$ , because the majority of matched sources are red.

3. Sources must have high-S/N 2MASS detections. We impose this limit by requiring  $J < 15.8$ ,  $H < 15.1$ , and  $K_s < 14.3$ , which corresponds to  $10\sigma$  detections. Since the majority of matched sources have  $J - K_s$  colors bluer than 1.5 (see below), the faint limit is in practice determined by the condition on  $K_s$  flux.

4. Sources must be unresolved in SDSS data. The SDSS star-galaxy separation is robust to  $r^* \sim 21.5$ , which is significantly fainter than the faint limit of the resulting sample, and only a negligible number of galaxies are likely to be present in the final sample.

These limits result in a sample of 13,924 sources. Note that the fourth condition does not necessarily exclude all extragalactic sources since QSOs are typically optically unresolved sources. However, low-redshift QSOs can be easily recognized in the SDSS  $g^* - r^*$  versus  $u^* - g^*$  color-color diagram (see Fig. 1) as shown by Fan (1999). There are

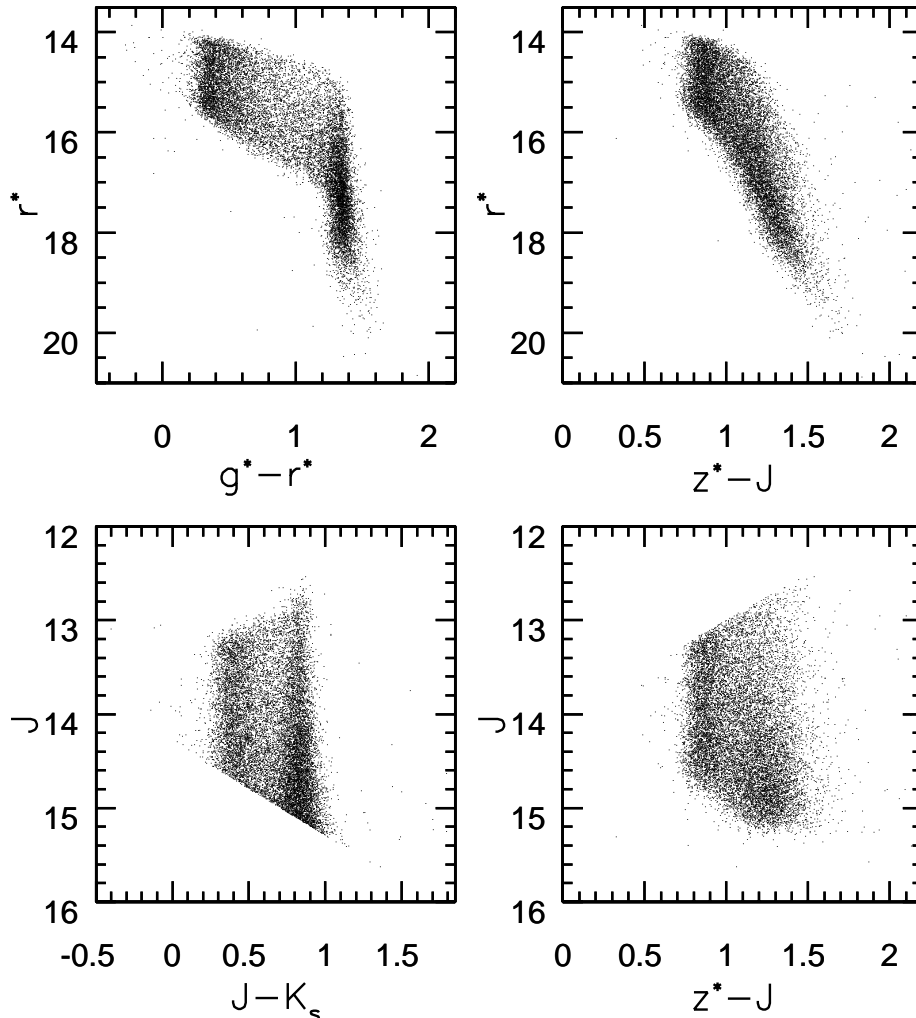


FIG. 4.—Color-magnitude diagrams for  $\sim 14,000$  stars with the smallest ( $\leq 10\%$ ) photometric errors in both surveys. The bright limit is determined by the saturation in SDSS data, and the faint limit is determined by the 2MASS sensitivity.

100 matched sources in this region of the color-color diagram, but only seven of these are bright enough to satisfy the (conservative) 2MASS S/N limits (condition 3 above). These sources, together with the optically classified galaxies, will be discussed in a separate publication.

Figure 4 displays color-magnitude diagrams for the 13,917 selected stellar sources. The SDSS and 2MASS photometry is better than 10% for the majority of this sample

due to the imposed cuts. The top left panel shows an  $r^*$  versus  $g^*-r^*$  diagram and can be compared with the analogous diagram for all SDSS sources displayed in the top left panel in Figure 1. The bright limit on the  $r^*$  magnitude is correlated with the  $g^*-r^*$  color because the red sources become saturated in SDSS data at a fainter  $r^*$  magnitude than the blue sources. Similarly, the faint limit depends even more strongly on the  $g^*-r^*$  color because only compara-

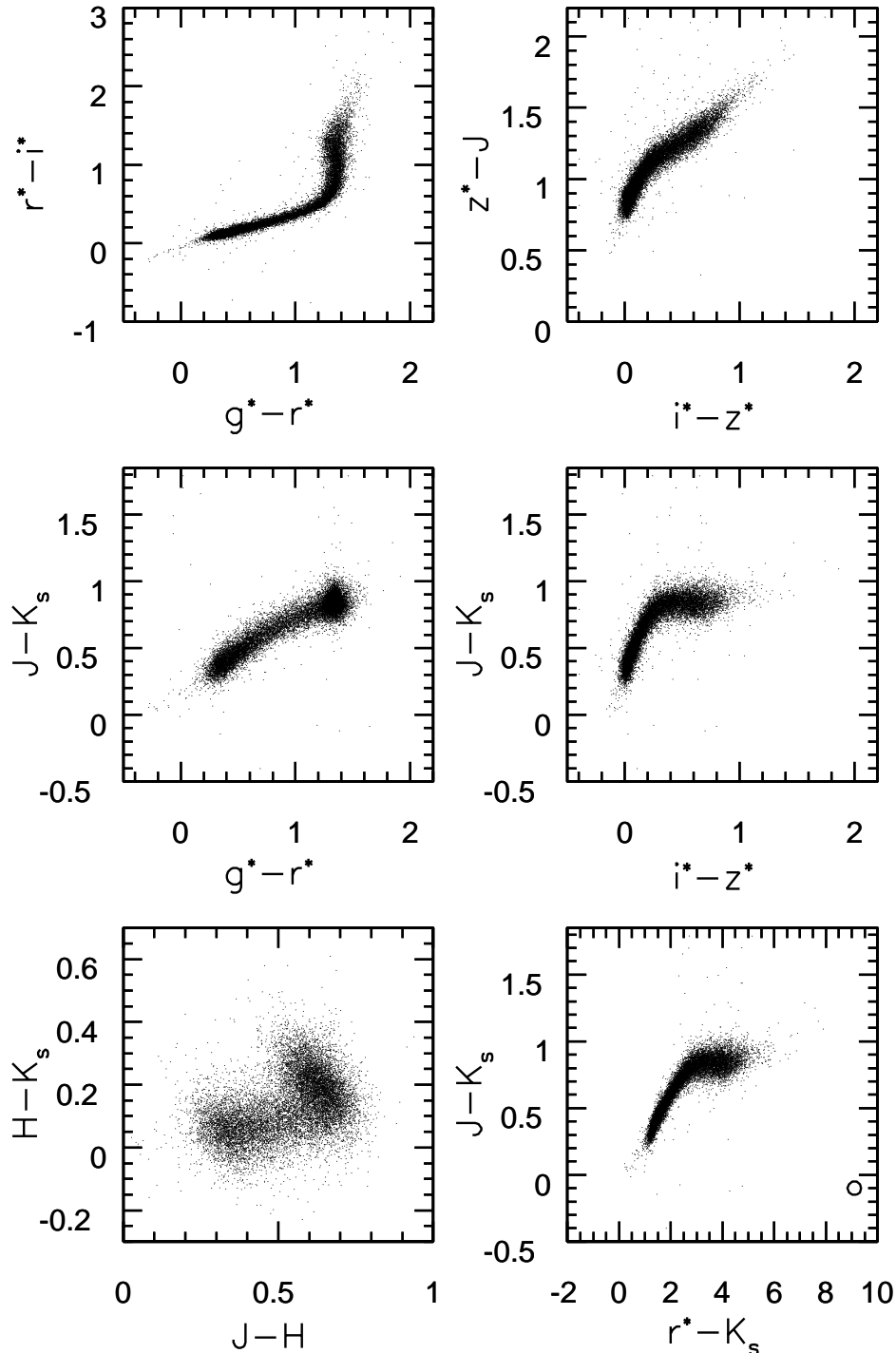


FIG. 5.—Color-color diagrams for the same stars shown in Fig. 4. The stellar locus is clearly visible in all diagrams that include at least one optical band. In the near-infrared color-color diagram, shown in the bottom left panel, the color ranges are much smaller, and consequently the stellar locus is not as well defined as in optical and optical-infrared color-color diagrams. The position of Gl 229B, the first discovered T dwarf (Nakajima et al. 1995), is marked by an open circle at  $r^*-K_s = 9.1$  and  $J-K_s = -0.1$  in the bottom right panel.

tively bright blue objects can pass the 2MASS faint limit cutoffs due to their steeply falling spectral energy distributions.<sup>22</sup> Essentially the same effects can be seen in the other three color-magnitude diagrams that combine optical and infrared data. Note the sharp faint limit in the  $J$  versus  $J - K_s$  diagram because it is determined by the  $K_s < 14.3$  condition, as discussed above.

<sup>22</sup> Due to these cutoffs, essentially all matched stars belong to the Galactic disk. With the aid of models discussed in § 5, we estimate that  $\sim 97\%$  of these stars are on main sequence.

The color-color diagrams for the selected subsample are shown in Figure 5. The top left panel shows an analogous diagram to the one displayed in the bottom left panel of Figure 1. Note that there is no significant difference in the appearance of the stellar locus. However, as is already visible in Figure 4, the matched sample has a larger fraction of red stars (see below). The following three panels show optical-infrared color-color diagrams. Note that the stellar locus is clearly visible in all of them, confirming that the optical and near-infrared broadband colors of normal stars can be described to within 0.1–0.2 mag in terms of temperature as a single parameter. In particular, the near-

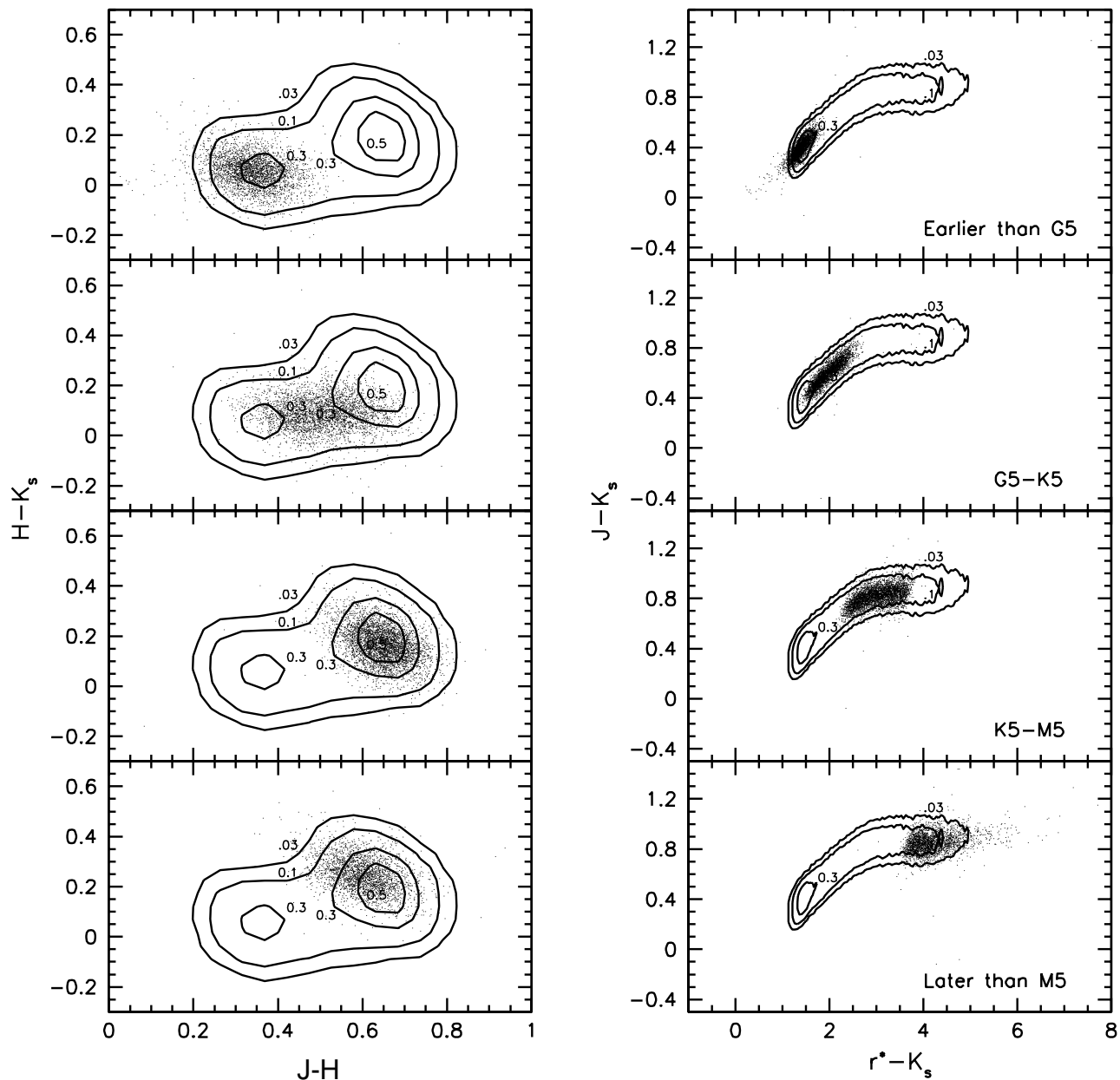


FIG. 6.—Distribution of stars in four optically selected subsamples, which trace the stellar spectral sequence in the  $H - K_s$  vs.  $J - H$  and  $J - K_s$  vs.  $r^* - K_s$  color-color diagrams. Stars in each subsample are shown as dots, and the distribution of the whole sample is shown by contours. The contour levels are 0.5, 0.3, 0.1, and 0.03 of the peak density. The top row includes stars with spectral types earlier than G5 (21% of the whole sample), the second row corresponds to spectral types between G5 and K5 (27%), the third row includes spectral types between K5 and M5 (32%), and the bottom row includes stars later than M5 (21%). See the electronic edition of the *Journal* for a color version of this figure.

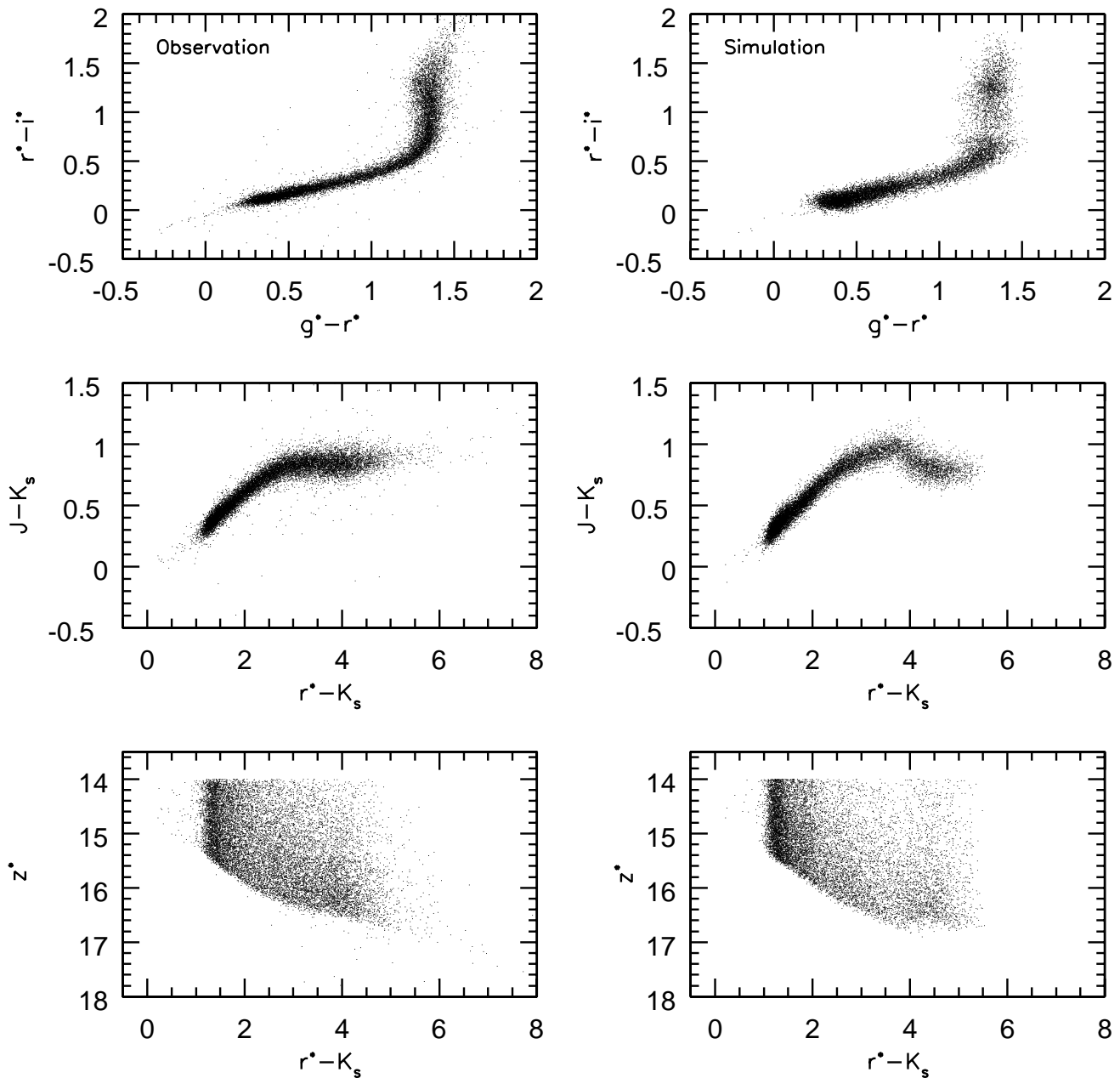


FIG. 7.—Comparison of data with the predictions of a stellar population synthesis code. The panels on the left show the diagrams for the matched objects, and those on the right show the simulated population. The top row compares optical colors, and the middle row shows an optical-infrared color-color diagram. The bottom row compares the  $z^*$  vs.  $r^* - K_s$  color-magnitude diagrams. See the electronic edition of the *Journal* for a color version of this figure.

infrared fluxes can be predicted for the majority of sources to 0.1–0.2 mag from the optical fluxes alone. However, the converse is not true; stars with varying optical colors may occupy the same region in near-infrared color-color diagrams (nota bene, in the Rayleigh-Jeans tail color is independent of temperature). This is true for some stars even in the case of optical-infrared color-color diagrams. For example, all M stars occupy a very small region in the  $J - K_s$  versus  $g^* - r^*$  diagram shown in the middle left panel ( $g^* - r^* = 1.4$ ,  $J - K_s = 0.85$ ). While their  $g^* - r^*$  color can be determined from their  $J - K_s$  color, it is impossible, for example, to constrain their  $r^* - i^*$  color, which can vary by more than a magnitude.

The bottom right panel displays the  $J - K_s$  versus  $r^* - K_s$  color-color diagram. This diagram was used by Kirkpatrick

et al. (1999) in their search for L dwarfs; we present it here as reference (note that Kirkpatrick et al. display this graph with reversed  $J - K_s$  axes). Kirkpatrick et al. show that the M spectral sequence begins around  $r^* - K_s = 2.0$ , and ends around  $r^* - K_s = 8.0$ , where the L dwarf sequence begins. L dwarfs are very rare and are not apparent on the diagram. The position of Gl 229B, the first discovered T dwarf (Nakajima et al. 1995), is marked by an open circle at  $r^* - K_s = 9.1$  and  $J - K_s = -0.1$ .

The bottom left panel shows a color-color diagram constructed from 2MASS data alone. The stellar locus is not as well defined as in the optical and optical-infrared color-color diagrams, and the position of a star in this diagram is not strongly correlated with its spectral type. However, the structure seen in the  $H - K_s$  versus  $J - H$  color-color

diagram indicates that there is at least a weak correlation between the spectral type and the position in this diagram. Understanding such a correlation could allow for very efficient studies of the Galactic disk structure based on only 2MASS data; unlike SDSS, 2MASS will extend over the entire sky. We attempt to quantify such a correlation by separating sources based on their optical colors, and then studying their distribution in the  $H - K_s$  versus  $J - H$  color-color diagram.

The  $r^* - i^*$  versus  $g^* - r^*$  color-color diagram can be used to separate the stars into rough spectral classes (see § 3.1). We divide the sample into:

1. Stars with spectral types earlier than G5 by the condition  $g^* - r^* \leq 0.5$ . There are 2894 stars (21%) in this subsample.
2. Stars with spectral types between G5 and K5:  $0.5 < g^* - r^* \leq 1.0$ . There are 3731 stars (27%) in this subsample.
3. Stars with spectral types between K5 and M5:  $g^* - r^* > 1.0$  and  $r^* - i^* \leq 1.0$ . There are 4393 stars (32%) in this subsample.
4. Stars with spectral types later than M5:  $g^* - r^* > 1.0$  and  $r^* - i^* > 1.0$ . There are 2873 stars (20%) in this subsample.

The distribution of stars in the  $H - K_s$  versus  $J - H$  and  $J - K_s$  versus  $r^* - K_s$  color-color diagrams is shown separately for each subsample in the four panels of Figure 6. The spectral types are plotted in the same order as listed above, with stars earlier than type G5 shown in the top panel. Stars from each optically selected spectral subsample are plotted as dots, and the contours represent the distribution of the whole sample. The contour levels are 0.5, 0.3, 0.1, and 0.03 of the peak density. The separation of the four classes is much better defined in the  $J - K_s$  versus  $r^* - K_s$  diagram, because the range of colors is much larger than in the  $H - K_s$  versus  $J - H$  diagram. The two peaks in the  $H - K_s$  versus  $J - H$  source distribution correspond to stars earlier than G5 (blue peak), and to stars with spectral types later than K5 (red peak). Stars with spectral types between G5 and K5 populate the area between the peaks, and the stars with spectral types later than M5 populate the region with the reddest  $J - K_s$  and  $r^* - K_s$  colors.

We have also attempted a finer binning in the  $r^* - i^*$  versus  $g^* - r^*$  color-color diagram and found that the 2MASS data alone does not allow for a more precise spectral classification than that presented in Figure 6. Nevertheless, we find that the 2MASS color  $J - K_s = 0.6$  provides a good overall separation of stars with  $g^* - r^* < 0.7$  from stars with  $g^* - r^* \geq 0.7$  (see Fig. 5). There are 5099 stars (37%) with  $g^* - r^* < 0.7$  in the subsample of 13,917 stars with good photometry, and 93% of these also have  $J - K_s < 0.6$ . Of the remaining 8818 stars with  $g^* - r^* \geq 0.7$ , there are 96% with  $J - K_s \geq 0.6$ . These numbers show that there is a  $\sim 95\%$  probability of success in predicting whether the SDSS  $g^* - r^*$  color is greater or smaller than 0.7 from the information specifying whether the 2MASS  $J - K_s$  color is greater or smaller than 0.6. The SDSS  $g^* - r^*$  color of 0.7 separates stars with spectral type earlier than K0 from stars with later spectral types. This boundary is fuzzy to within two to three spectral subtypes due to the effects of varying metallicity and gravity on stellar colors. Such a method of separating early from late type stars may

prove useful in selecting subsamples of 2MASS data for the studies of Galactic disk structure.

## 5. COMPARISON OF DATA WITH A STELLAR POPULATION SYNTHESIS CODE

We compare the number counts and the source distribution in color-color diagrams using the code of Fan (1999, hereafter F99) for simulating SDSS observations of unresolved sources, which we have extended to the 2MASS bands (Finlator 2000). F99 compared several simulated stellar populations to data obtained by the ESO Imaging Survey Patch B (Prandoni et al. 1998) and found that the position of the simulated stellar locus in SDSS color-color space agreed very well with the data. Nevertheless, he also found that the number counts could differ by up to  $\sim 20\%$ . In the following section we present an expanded analysis of the model predictions, made possible by the new 2MASS and SDSS data, and discuss similar discrepancies. Detailed discussion of this model is given by F99, and here we only provide a brief summary.

### 5.1. Generating a Simulated Population

The population synthesis code for generating a simulated stellar population at a given Galactic latitude and longitude is based on the following inputs/steps.

1. A Galactic structure model based on the star count models of Bahcall & Soneira (1981, 1984) is used to generate the number of halo and disk stars as a function of Galactic latitude and longitude. The disk scale height is assumed to increase with stellar age (i.e., the scale height is correlated with the spectral type), and the Galactic halo is flattened. The initial mass function is taken from Haywood, Robin, & Cr ez e (1997) and is assumed to be valid both for disk and halo stars.

2. To generate the properties of a specified stellar population, the simulation generates the mass, age, and metallicity of each star with the aid of the Padova stellar evolutionary tracks and isochrones (Bertelli et al. 1994). The resulting  $T_{\text{eff}}$ ,  $[\text{Fe}/\text{H}]$ , and  $\log g$  are then used to select a stellar atmosphere model in order to determine the colors for each star.

3. The hybrid model stellar atmospheres compiled by Lejeune, Buser, & Cuisinier (1997a, 1997b) are used to compute the SDSS and 2MASS colors of stars, given their effective temperature  $T_{\text{eff}}$ , metallicity  $[\text{Fe}/\text{H}]$ , and surface gravity  $\log g$ .

4. The SDSS AB magnitudes are computed as described in F99, and the 2MASS Vega magnitudes,  $m$ , are computed using

$$m = -2.5 \log \frac{\int d(\log \nu) f_\nu S_\nu}{\int d(\log \nu) S_\nu} - 48.60 + m_0, \quad (1)$$

where  $m_0(J) = -0.89$ ,  $m_0(H) = -1.37$ , and  $m_0(K_s) = -1.84$  represent the offsets from the AB magnitude system. These offsets were computed by assuming that the flux from Vega is constant within any 2MASS band and equal to 1595, 1024, and 667 Jy in the  $J$ ,  $H$ , and  $K_s$  bands, respectively (M. Cohen 2000, private communication).

5. Photometric errors in SDSS bands are added as described in Appendix A of F99. The 2MASS photometric errors are derived from an on-line plot of photometric

repeatability versus magnitude.<sup>23</sup> Errors are  $\sim 0.03$  mag at the bright end, and then rise to  $\sim 0.1$  mag at  $J = 15.8$ ,  $H = 15.1$ ,  $K_s = 14.3$ .

### 5.2. Comparison of Simulated Observations with the Data

Figure 7 compares the photometric properties of the matched sources with a population simulated at  $(l, b) = (150^\circ, -60^\circ)$  (the properties of a sample are strong functions of the Galactic coordinates) and spanning the same area on the sky ( $47.41 \text{ deg}^2$ ). The panels on the left show the dia-

grams for the matched objects, and those on the right show the simulated population. To ensure the same selection effects for both samples, we require that the model fluxes satisfy  $z^* > 14$ ,  $J < 15.8$ ,  $H < 15.1$ , and  $K_s < 14.3$ . These conditions result in 12,740 simulated sources, only 9% fewer than the observed value of 13,917 matched sources. Since the selection effects are quite complicated and include two independent surveys, this close agreement is quite encouraging. We note that the simulated population does not include “exotic” objects such as white dwarfs and QSOs.

The top row in Figure 7 compares optical colors. The overall agreement is satisfactory, although there are fewer simulated stars with  $r^* - i^* \sim 0.8 - 0.9$ , yielding a discontinuity in the stellar locus in the  $g^* - r^*$  versus  $r^* - i^*$  diagram.

<sup>23</sup> Available at <http://www.ipac.caltech.edu/2mass/releases/second/doc/figures/secii2f7.gif>.

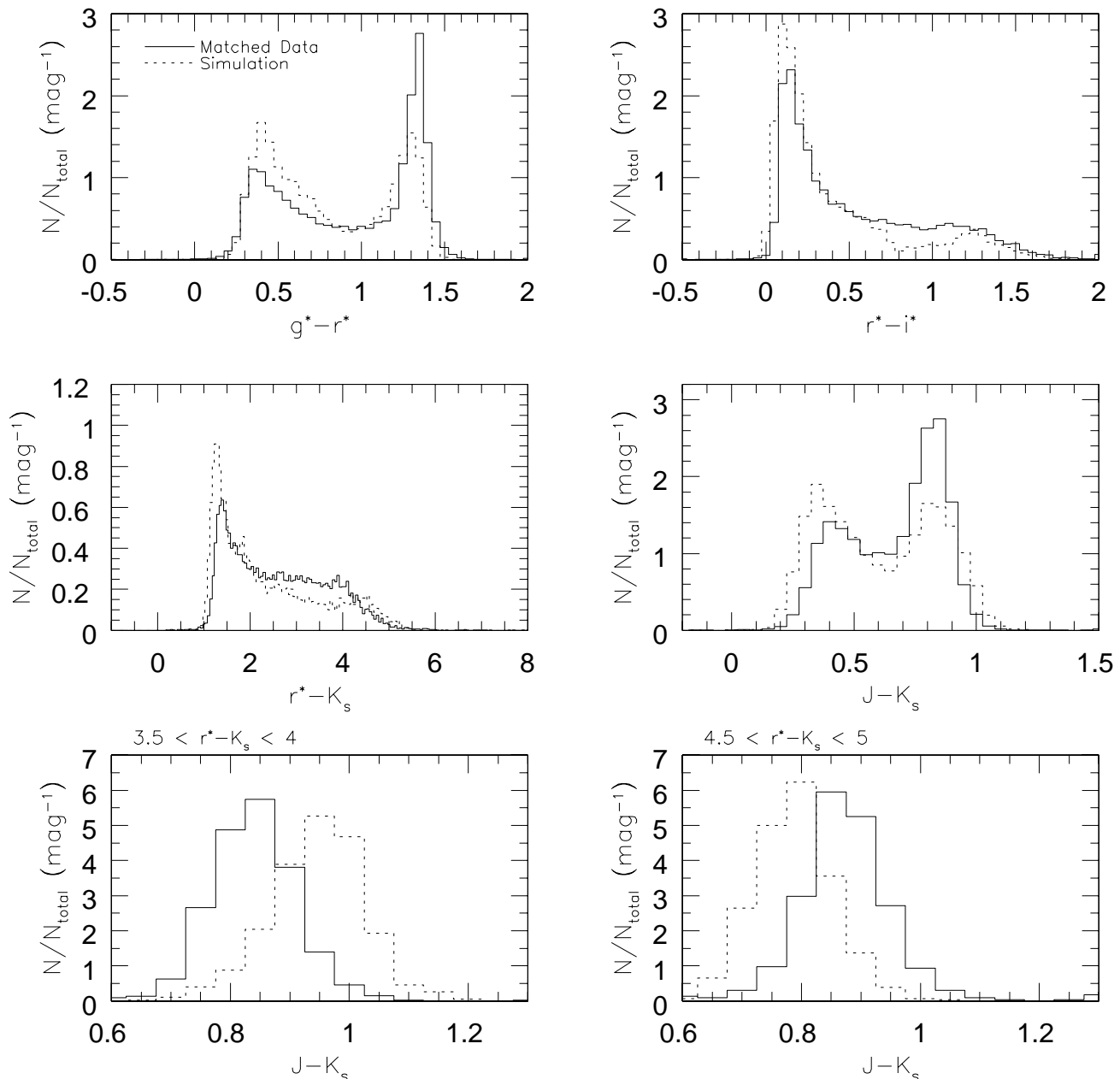


FIG. 8.—Various color probability distributions for the matched and simulated objects shown in Fig. 7. The top four panels show that the simulation overestimates the overall counts of blue stars while underestimating the redder star counts. The bottom two panels show the  $J - K_s$  color distributions for two subsamples of M stars: the left panel shows stars with  $3.5 < r^* - K_s < 4$  ( $\sim M3$ ) and the right panel shows stars with  $4.5 < r^* - K_s < 5$  ( $\sim M5$ ). Note that the  $J - K_s$  colors for simulated early-M stars are significantly redder (0.15 mag) than observed, while they are bluer than observed for the mid- to late-M stars. See the electronic edition of the *Journal* for a color version of this figure.

This is due to the different model libraries used for objects with  $T_{\text{eff}} > 3500$  K and  $T_{\text{eff}} < 3500$  K, as discussed by F99. The middle row in Figure 7 shows an optical-infrared color-color diagram. The overall morphology is well reproduced by the simulated population, except for the M stars ( $r^* - K_s \gtrsim 3$ ), which have notably different colors. While the observations suggest that infrared colors should not vary with  $r^* - K_s$  color for  $r^* - K_s \gtrsim 3$ , the simulated M stars become bluer in  $J - K_s$  after this point. We will further discuss this discrepancy below. The bottom row in Figure 7 compares the  $z^*$  versus  $r^* - K_s$  color-magnitude diagrams. Again, the overall morphology is reproduced, but the simulation does not seem to generate enough bright stars with intermediate  $r^* - K_s$  colors.

To provide a more quantitative comparison of the data with the models, we display histograms of the matched and simulated objects in Figure 8. The top four plots show that the simulation overestimates the overall counts of blue stars while underestimating the red star counts. While the observed ratio of stars redder and bluer than  $J - K_s = 0.6$  is 1.73, the simulated ratio is 0.98. The top right panel clearly shows the lack of simulated stars with  $r^* - i^* \sim 0.8 - 0.9$  mentioned earlier.

The disagreement between the observed and simulated ratio of red to blue stars could be due either to incorrect parameters of the Galactic structure model or to an incorrect shape of the initial mass function employed in the simulation. The blue stars have higher luminosities than do the red stars and thus are observed to larger distances. The majority of simulated red stars with  $J - K_s > 0.6$  have distances ranging from 200 to 800 pc (median value of 500 pc), while the majority of blue stars are in the distance range 800–2000 pc (median value of 1000 pc). Decreasing the disk scale height for red stars and increasing it for blue stars in the expression for stellar density as a function of distance from the Galactic plane (F99, eqs. [5] and [6]) can increase the simulated ratio of red to blue stars. However, these adjustments would involve changing the age of stars, resulting in a change in the total number of simulated stars.

Similarly, one can increase the simulated ratio of red to blue stars by increasing the slope of the initial mass function (IMF) at the low-mass end. The simulated sample is dominated by stars with masses  $\lesssim 1 M_{\odot}$ . The majority of stars with  $J - K_s > 0.6$  have masses between  $0.3 M_{\odot}$  and  $0.75 M_{\odot}$ , while the stars with  $J - K_s < 0.6$  have masses between  $0.75 M_{\odot}$  and  $1.1 M_{\odot}$ . In this mass range, the simulation adopts  $dN/dM \propto M^{-1.7}$ . We have examined a set of models with  $dN/dM \propto M^{-n}$  and found that  $n = 2.5 \pm 0.1$  produces the observed ratio of red to blue stars. However, the total number of stars becomes too low and another model adjustment is needed. Thus, to meaningfully constrain the free parameters requires an extensive modeling effort beyond the scope of this work. A detailed analysis of SDSS stars counts and their implications for the Galactic structure model will be reported in Chen et al. (2000).

Another model difficulty is related to the properties of the stellar models, as opposed to the Galactic distribution of stars. As discussed above, the  $J - K_s$  colors of simulated M stars becomes bluer for  $r^* - K_s \gtrsim 3$ , while the observations suggest that they should stay constant at roughly 0.85. The bottom two panels of Figure 8 show the  $J - K_s$  histograms for two subsamples of M stars: the left panel shows stars with  $3.5 < r^* - K_s < 4$  ( $\sim M3$ ), and the right panel shows stars with  $4.5 < r^* - K_s < 5$  ( $\sim M5$ ). It is evident that the

$J - K_s$  color for simulated early M stars is significantly redder (0.15 mag) than observed, while it is bluer than observed for the mid-to late-M stars. Such discrepancies between the data and simulations for M stars are not surprising because these stars are notoriously difficult to model due to their complicated chemistry (Allard et al. 1997). Particularly problematic are incomplete and uncertain opacity tables, as well as the possibility of dust condensation in the outer cool parts of the atmosphere, an effect which is usually ignored.

## 6. CONCLUSIONS

This preliminary study indicates the enormous potential of combined 2MASS and SDSS data for stellar and Galactic structure studies. The results of the positional matching of sources presented here indicate that both surveys will provide outstanding astrometry ( $\sim 0.1$  rms per coordinate) for an unprecedented number of objects. Eight-color accurate photometry (better than 0.1 mag) for millions of stars is bound to place studies of stellar and Galactic structure and evolution at an entirely new level. Such a large number of stars will enable detailed studies of the stellar initial mass function and its possible Galactic variation, of the metallicity gradients in the Galaxy, and similar other types of analyses, which were until now impeded by the lack of large and reliable data sets. For example, by analyzing sources from less than 1% of the final 2MASS-SDSS overlapping area, we find that either the parameters of the standard Galactic structure model or the conventional initial mass function must be changed to make simulations fit the data. Also, the wide and detailed spectral coverage based on eight fluxes provides strong tests for the stellar structure and atmosphere models. As we have shown here, the near-infrared model colors for M dwarfs are significantly different from the observed colors.

In addition to the testing of stellar and Galactic structure models as discussed here, such a large and uniform data set is ideal for discovering objects with unusual colors (e.g., T Tau stars, Herbig Ae/Be stars, brown dwarfs, etc.). An analysis of such outliers in color-color space will be presented in a forthcoming publication.

We are grateful to Martin Cohen and Mike Skrutskie for providing to us 2MASS transmission curve data and for helpful discussions. This publication makes use of data products from the Two Micron All Sky Survey, which is a joint project of the University of Massachusetts and the Infrared Processing and Analysis Center/California Institute of Technology, funded by the National Aeronautics and Space Administration and the National Science Foundation. The Sloan Digital Sky Survey (SDSS)<sup>24</sup> is a joint project of The University of Chicago, Fermilab, the Institute for Advanced Study, the Japan Participation Group, The Johns Hopkins University, the Max-Planck-Institute for Astronomy, Princeton University, the US Naval Observatory, and the University of Washington. Apache Point Observatory, site of the SDSS, is operated by the Astrophysical Research Consortium. Funding for the project has been provided by the Alfred P. Sloan Foundation, the SDSS member institutions, the National Aeronautics and Space Administration, the National Science Foundation, the Department of Energy, and Monbuscho, Japan.

<sup>24</sup> The SDSS Web site is <http://www.sdss.org/>.

## REFERENCES

- Allard, F., Hauschild, P. H., Alexander, D. R., & Starrfield, S. 1997, *ARA&A*, 35, 137
- Bahcall, J. N., & Soneira, R. M. 1981, *ApJS*, 47, 357
- . 1984, *ApJS*, 55, 67
- Becker, R. H., White, R. L., & Helfand, D. J. 1995, *ApJ*, 450, 559
- Bertelli, G., Bressan, A., Chiosi, C., Fagotta, F., & Nasi, E. 1994, *A&AS*, 106, 275
- Chen, B., et al. 2001, in preparation
- Fan, X. 1999, *AJ*, 117, 2528 (F99)
- Fan, X., et al. 1999, *AJ*, 118, 1
- Finlator, K. 2000, Senior thesis, Princeton Univ.
- Fukugita, M., Ichikawa, T., Gunn, J. E., Doi, M., Shimasaku, K., & Schneider, D. P. 1996, *AJ*, 111, 1748
- Gunn, J. E., et al. 1998, *AJ*, 116, 3040
- Haywood, M., Robin, A. C., & Cr ez e, M. 1997, *A&A*, 320, 428
- Ivezi c, Z., et al. 2000, *AJ*, 120, 963
- Kirkpatrick, J. D., et al. 1999, *ApJ*, 519, 802
- Krisciunas, K., Margon, B., & Szkody P. 1998, *PASP*, 110, 1342
- Leggett, S. K., et al. 2000, *ApJ*, 536, L35
- Lejeune, T., Buser, R., & Cuisinier, F. 1997a, *A&AS*, 125, 229
- . 1997b, *A&AS*, 130, 65
- Lenz, D. D., Newberg, J., Rosner, R., Richards, G. T., & Stoughton, C. 1998, *ApJS*, 119, 121
- Lupton, R. H., Gunn, J. E., & Szalay, A. 1999, *AJ*, 118, 1406
- Lupton, R. H. et al. 2001, in preparation
- Nakajima, T., Oppenheimer, B. R., Kulkarni, S. R., Golimowski, D. A., Matthews, K., & Durrance, S. T. 1995, *Nature*, 378, 463
- Oke, J. B., & Gunn, J. E. 1983, *ApJ*, 266, 713
- Pier, J. R., et al. 2001, in preparation
- Prandoni, I., et al. 1999, *A&A*, 345, 448
- Schlegel, D., Finkbeiner, D. P., & Davis, M. 1998, *ApJ*, 500, 525
- Skrutskie, M. F., et al. 1997, *The Impact of Large-Scale Near-IR Sky Surveys*, ed. F. Garz n, N. Epchtein, A. Omont, B. Burton, & P. Persei (Dordrecht: Kluwer), 25
- Yanny, B., et al. 2000, *ApJ*, 540, 825
- York, D. G., et al. 2000, *AJ*, submitted